# Carbon Nanofiber Aerogel Converted from Bacterial Cellulose for Kilohertz AC-Supercapacitors

Nazifah Islam<sup>1</sup>, Md Nadim Ferdous Hoque<sup>1</sup>, Yujiao Zu<sup>2</sup>, Shu Wang<sup>2</sup> and Zhaoyang Fan<sup>1</sup>

# ABSTRACT

Compact-size kilohertz (kHz) AC-supercapacitors are being pursued for ripple current filtering and pulsed energy storage. However, their development is limited by a small areal capacitance density due to very thin electrode used for meeting frequency requirement. In our work, crosslinked carbon nanofiber aerogel (CCNFA) was investigated as freestanding electrode for kHz AC-supercapacitors with an areal capacitance density as large as 4.5 mF cm² at 120 Hz, 5-10 times larger than most reports. The CCNFA was obtained in a rapid plasma carbonization process of bacterial cellulose. The fabrication route adopted here is simple and straightforward, and the produced CCNFA electrode was found to be very suitable for high-frequency AC-supercapacitors. The operating voltage range of CCNFA based AC-supercapacitors can be expanded to 3 V by utilizing an organic electrolyte. In addition to AC-Supercapacitor performance, the morphology and material properties of bacterial cellulose aerogel and CCNFA were also reported.

# INTRODUCTION

The conventional supercapacitors have a frequency response limited below 1 Hz, or they only work under DC current and therefore cannot be used for current ripple filtering. In contrast, AC-Supercapacitor should have a frequency response above kHz so that they can be used as a filtering capacitor to replace bulky aluminium electrolytic capacitors in common power electronic applications such as line-frequency AC/DC conversion. Both high capacitance density and kilohertz frequency response are crucial for AC-supercapacitor [1]. Great progresses are being achieved by exploring different carbon nanostructures [2-7], but the reported areal capacitance is still low for practical applications. Although fast pseudocapacitors were also reported with large capacitance [8], they are intrinsically slower than double layer capacitors and cannot work at kHz frequencies.

Large capacitance of supercapacitors arises from a large surface area of porous carbon, however, the complex pore structure renders them incapable for fast mass transport in electrolyte. For AC-supercapacitors, the structure of the electrode must be carefully tailored to ensure fast mass transport, high electronic conductivity as well as a reasonable

<sup>&</sup>lt;sup>1</sup> Department of Electrical and Computer Engineering and Nano Tech Center, Texas Tech University, Lubbock, TX 79409, U.S.A.

<sup>&</sup>lt;sup>2</sup> Department of Nutritional Sciences, Texas Tech University, Lubbock, TX 79409, U.S.A.

surface area. These properties are predominantly controlled by the choice of precursor material and the process of carbonization.

In this work, we converted bacterial cellulose (BC), a well-known carbon nanofiber precursor with ultrathin (50 nm or less) fiber [9], to CCNFA with large specific surface area and suitable pore size. We demonstrated that adopting high-temperature plasma pyrolysis technique to produce CCNFA from BC aerogel, is essential to deliver kHz speed while maintaining a large areal capacitance. The KHz AC-supercapacitor performances were then investigated in aqueous and organic electrolytes [10].

# **EXPERIMENT**

BC pellicles were obtained from Kombucha strains by fermentation process [11]. The pellicles were washed in NaOH and NaOCl solutions to remove impurities. The clean pellicles were freeze dried at -80°C to get BC nanofiber aerogel. Carbon nanofiber aerogel were obtained by pyrolyzing the BC aerogel under high temperature. Three different pyrolysis processes were examined: conventional furnace based thermal pyrolysis at 800°C for 2 hours under Ar flow (Ar-CCNF); plasma pyrolysis under hydrogen flow (HP-CCNF) and plasma pyrolysis under flow of hydrogen and methane (HCP-CCNF). For plasma pyrolysis, a PECVD chamber was used. The substrate temperature for plasma pyrolysis was set at 750°C, which rapidly increased to >1200°C during plasma exposure. The plasma exposure duration was 15 minutes. In case of hydrogen-methane gas mixture, the precursor cellulose film was sandwiched between two graphite foils to avoid growth of graphene nanosheets on the fibers [12].

The carbon fiber materials were characterized by scanning electron microscopy (SEM), transmission electron microscopy (TEM) and X-ray photoelectron spectroscopy (XPS). Electrochemical capacitive performances were investigated by assembling symmetric coin cells using the CCNFA as electrodes. 6 M KOH in water and 1 M TEABF $_4$  in acetonitrile solutions were employed as aqueous and organic electrolytes, respectively. Electrochemical measurements were conducted using an electrochemical workstation. Electrochemical impedance spectroscopy (EIS) was measured from 100 kHz to 1 Hz with a sinusoidal AC voltage of 10 mV amplitude. Cyclic voltammetry (CV) was carried out in the range of 0–0.9 V for aqueous electrolyte cells and in 0–2.5 V for organic electrolyte cells at different scan rates up to 1000 V s $^{-1}$ .

# DISCUSSION

When carbon material is derived from pyrolysis of carbon precursors, the pyrolysis conditions critically affect the material properties of the derived carbon, including surface morphology, electrical conductivity, crystalline states etc. [13], and these properties principally determine the capacitance and response speed achievable from the carbon. BC derived carbon nanofibers were previously reported as supercapacitor electrodes, but those are for conventional supercapacitors with DC response [14-16]. To find the suitable condition for kHz response, we explored 3 different conditions, as mentioned in the experimental section. The plasma pyrolysis method was chosen particularly for some specific advantages over the conventional furnace based thermal pyrolysis technique. Plasma ignition can produce a much higher temperature within a certain area which is almost impossible to obtain by electrical or other heating methods. The degree of graphitization and hence the electrical conductivity of the carbonized species are improved with increased temperature. Besides, the plasma technique is a very rapid

process, scaling down the material preparation time to one tenth or even less compared to the thermal process.

The morphologies of derived carbon fibers were studied by SEM (Fig. 1 a-c). The conventional furnace based pyrolysis technique is known to create micropores on the fibers, which have detrimental effect on movement of electrolyte and ions, hence limiting the response time. When hydrogen gas alone is employed in the plasma pyrolysis, the etching effect is obvious (Fig. 1b) from the damaged fiber walls and broken branches. Instead of inert  $N_2$  or Ar, hydrogen is more effective for removal of oxygen containing groups from the carbon precursor. However, at the high temperature, hydrogen is found to become too reactive to even corrode the carbon itself, which is undesired. To balance this effect, a hydrocarbon gas, methane, was employed along with hydrogen. Compared

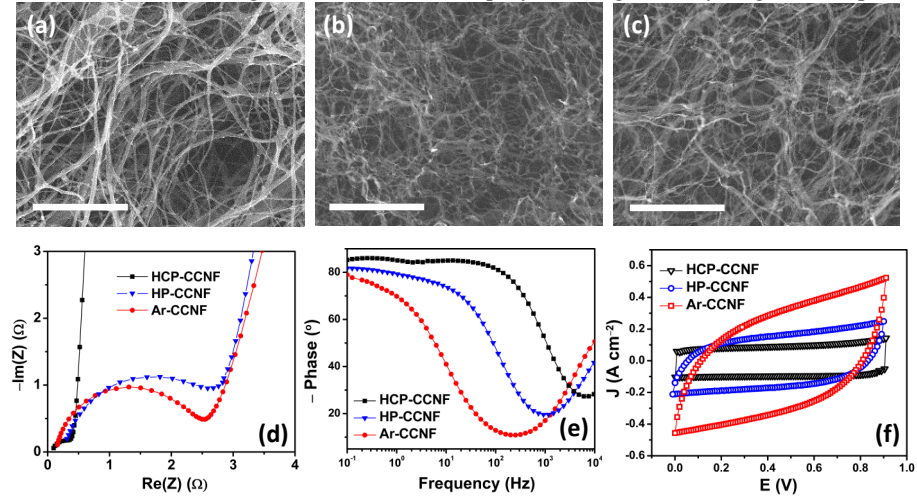


Figure 1. SEM images of HCP-CCNF (a), HP-CCNF (b) and Ar-CCNF (c). Scale bar:1 µm. (d) Nyquist impedance curves, (e) Bode phase spectra and (f) cyclic voltammetry plots of electrochemical capacitors.

to HP-CCNF, the HCP-CCNF is found to have a good crosslinked structure with solid fibers. The presence of the hydrocarbon, presumably, prevents the hydrogen from etching away the carbon. Moreover, in presence of methane, the temperature during plasma exposure is higher than hydrogen alone [10].

The three pyrolysis products were tested for the response speed in KOH aqueous electrolyte. The Nyquist impedance plot presented showed large semicircles for Ar-CCNF and HP-CCNF, indicating large electrolyte diffusion resistance. The phase spectra are presented in Fig. 1(e), which clearly demonstrates the discernible contrast among the 3 electrode materials under study. Ar-CCNF has characteristic frequency less than 10 Hz, HP-CCNF has around 100 Hz and HCP-CCNF is above 1 kHz. One set of representative cyclic voltammetry plots measured at 50 V s<sup>-1</sup> is presented for comparison. At this relatively slow scan rate, only the HCP-CCNF can maintain the desired rectangular shape. This experiment undoubtedly demonstrates the HCP-CCNF as the potential material for high speed supercapacitors.

The morphologies of BC and HCP-CCNF were further analyzed by TEM. Corresponding SEM and TEM images of BC nanofibers are presented in Fig. 2 (a, b) and those of HCP-CCNF are in Fig. 2 (d-f). Both SEM and TEM images, before and after carbonization, reveal the characteristic crosslinked pattern of the nanofibers. From the TEM of HCP-CCNF, the absence of micropores on the carbon fibers is apparent. From

SEM, it also noticeable that the dense BC network was converted to relatively open CCNF matrix, with a mass reduction of more than 95% during carbonization. The micron sized voids allow absorption of electrolytes throughout the electrode thickness and rapid motion of electrolyte ions during operation.

XPS survey scan was performed to monitor the degree of carbonization. Typically, cellulose and other similar hydrocarbon polymer compounds contain a significant amount of oxygen in forms of different functional groups. During carbonization, these functional groups decompose, and oxygen is released leaving the carbon chain. For a carbonized product, the oxygen content should be considerably small, although not completely diminished. In Fig. 2(c), the XPS survey data of BC and

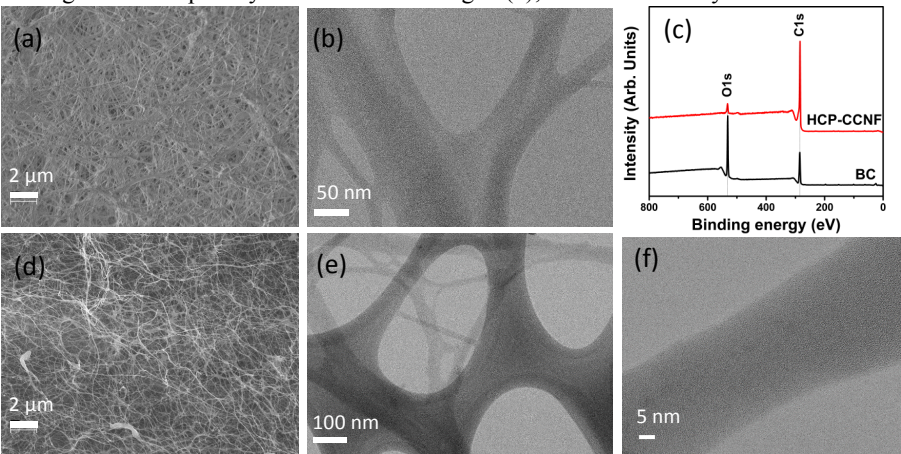


Figure 2. (a) SEM and (b) TEM of BC aerogel. (c) XRD pattern of BC aerogel. (d) SEM and (e, f) TEM images of HCP-CCNF.

HCP-CCNF are presented. The BC spectra shows presence of large amount of oxygen (O1s) which is even almost twice of the carbon content (C1s). After pyrolysis, the oxygen peak is suppressed to less than 10% of the C1s. The clearly dominating C1s peak confirms the superior quality of carbonization.

For electrochemical studies, three different thicknesses BC aerogel were taken for carbonization. After carbonization, the thicknesses were measured to be approximately 10  $\mu$ m, 20  $\mu$ m and 60  $\mu$ m. According to the thicknesses, the three electrodes were named as CCNF-10, CCNF-20 and CCNF-60, respectively. The capacitive performances relative to thicknesses are summarized in Fig. 3(a). The cutoff frequencies, defined when the phase angle reach – 45°, in aqueous electrolyte have been found to be 4.10, 3.30 and 1.35 kHz, for CCNF-10, 20 and 60, respectively, while maintaining a phase angle at or above 80 degrees at 120 Hz for all 3 samples. The capacitance increases from 1.51 mF cm<sup>-2</sup> for CCNF-10 to 4.5 mF cm<sup>-2</sup> for CCNF-60. The organic counterpart shows rather sluggish response, only the CCNF-10 demonstrates kHz frequency and 80° phase angle at 120 Hz. The capacitance densities are measured as 0.5, 1.08 and 2.55 mF cm<sup>-2</sup>, for CCNF-10, 20 and 60, respectively. KHz frequency response was observed with CCNF-10, with 1.8 kHz cutoff and -80° phase angle.

As examples, Nyquist plot and Bode plot of the impedance spectra of CCNF-60 in aqueous electrolyte and CCNF-10 in organic electrolyte are presented in Fig. 3 (b) and 3(c). The equivalent series resistance (ESR) and the electrolyte diffusion resistance (EDR), are critical parameters determining supercapacitor performance at higher frequencies.

From the Nyquist plot in Fig. 3(b), for aqueous cell, the ESR is  $0.013~\Omega~cm^2$  and the diffusion resistance (EDR) is  $0.054~\Omega~cm^2$ . These low resistance values prove the excellent electronic and ionic conduction properties of the CCNF matrix. For organic cells, the ESR and EDR are  $0.09~\Omega~cm^2$  and  $0.34~\Omega~cm^2$ , respectively.

Cyclic voltammetry plots of aqueous (Fig. 3 d) and organic electrolyte (Fig. 3 e) based cells at different scan rates are presented. In organic electrolyte, the achievable potential window can be expanded to 2.5-3 V [10], due to larger dissociation potential of acetonitrile. From the CV plots, the retention of capacitance with increased scan rates is clear from the nearly overlapped curves for both electrolytes. Moreover, the quasi rectangular shapes of the curves reinforce the claim of capacitive performance at

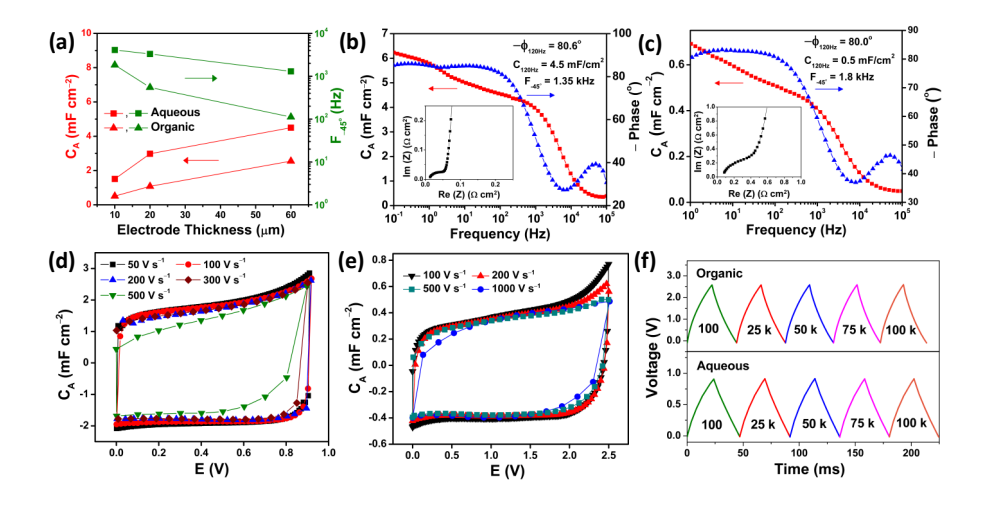


Figure 3. (a) Capacitance and frequency response data depending on electrode thickness. Impedance spectra of CCNF-60 electrodes in aqueous electrolyte (b) and CCNF-10 in organic electrolyte (c). Cyclic voltammograms of CCNF-20 electrode in aqueous electrolyte (d) and CCNF-10 electrode in organic electrolyte (e). (f) Cycling stability test of aqueous and organic electrolyte based capacitors.

ultrahigh rates. Fig. 3 (f) shows several representative Galvanostatic charge-discharge cycles. The charge-discharge cycling tests up to 100 k cycles for both aqueous and organic cells show little deviation, revealing electrochemical stability of the CCNF electrodes.

#### CONCLUSIONS

We demonstrated that the pyrolysis process has critical effect on the obtained CCNF properties, resulting different electrode response. Using a rapid plasma pyrolysis process in Ar and  $\rm H_2$ , we demonstrated the derived CCNF aerogel is suitable as electrode for developing kHz AC-supercapacitors with extremely large areal capacitance at 120 Hz in aqueous electrolyte. Their voltage operation window can be further increased to  $\sim 3$  V when an organic electrolyte used. Their excellent performance is attributed to the suitable pore size and well-crosslinked nanofiber structure of CCNF aerogel that can simultaneously offer a high ionic conductivity for the electrolyte in the porous electrode, a high electronic conductivity and a large surface area, resulting in high frequency response and large areal capacitance.

## **ACKNOWLEDGMENTS**

Funding from the National Science Foundation (1611060) is greatly acknowledged.

### REFERENCES

- [1] Z. Fan, N. Islam and S. B. Bayne, *Nano Energy* **39**, 306-320 (2017).
- [2] M. Cai, R. A. Outlaw, R. A. Quinlan, D. Premathilake, S. M. Butler and J. R. Miller, ACS Nano 8, 5873-5882(2014).
- [3] G. Ren, X. Pan, S. Bayne and Z. Fan, Carbon 71, 94-101 (2014).
- [4] Y. Yoo, S. Kim, B. Kim, W. Kim, J. Mater. Chem. A, 3, 11801-11806 (2015).
- [5] G. Ren, S. Li, Z. X. Fan, M. N. F. Hoque and Z. Fan, J. Power Sources 325, 152-160 (2016).
- [6] M. Zhang, Q. Zhou, J. Chen, X. Yu, L. Huang, Y. Li, C. Li and G. Shi, Energy Environ. Sci. 9, 2005-2010(2016).
- [7] N. Islam, J. Warzywoda and Z. Fan, Nano-Micro Lett. 10, 9 (2018). DOI: 10.1007/s40820-017-0162-4
- [8] X. Pan, G. Ren, M. N. F. Hoque, S. Bayne, K. Zhu and Z. Fan, Adv. Mater. Interfaces 1 (9), 1400398 (2014).
- [9] S. Li, J. Warzywoda, S. Wang, G. Ren and Z. Fan, Carbon 124, 212-218 (2017).
- [10] N. Islam, S. Li, G. Ren, Y. Zu, J. Warzywoda, S. Wang and Z. Fan, Nano Energy 40, 107-114 (2017).
- [11] C. Zhu, F. Li, X. Zhou, L. Lin and T. Zhang, J. Biomed. Mater. Res. Part A 102, 1548-1557 (2014).
- [12] X. Pan, K. Zhu, G. Ren, N. Islam, J. Warzywoda and Z. Fan, J. Mater. Chem. A 2, 12746-12753 (2014).
- [13] S. Li, T. Mou, G. Ren, J. Warzywoda, Z. Wei, B. Wang and Z. Fan, J. Mater. Chem. A 5, 1650-1657 (2017).
- [14] G. Zu, J. Shen, L. Zou, F. Wang, X. Wang, Y. Zhang and X. Yao, Carbon 99 (2016) 203-211.
- [15] X. Wang, D. Kong, Y. Zhang, B. Wang, X. Li, T. Qiu, Q. Song, J. Ning, Y. Song and L. Zhi, Nanoscale 8, 9146-9150 (2016).
- [16] J. Cai, H. Niu, Z. Li, Y. Du, P. Cizek, Z. Xie, H. Xiong and T. Lin, ACS Appl. Mater. Interfaces 7, 14946-14953 (2015).